WATER RESOURCES RESEARCH, VOL. 35, NO. 3, PAGES 651–662, MARCH 1999

Permeability of shaly sands

A. Revil[1] and L. M. Cathles III

Global Basin Research Network Group, Department of Geological Sciences, Cornell University, Ithaca, New York

Abstract. The permeability of a sand shale mixture is analyzed as a function of shale fraction and the permeability of the two end-members, i.e., the permeability of a clay-free sand and the permeability of a pure shale. First, we develop a model for the permeability of a clay-free sand as a function of the grain diameter, the porosity, and the electrical cementation exponent. We show that the Kozeny-Carman-type relation can be improved by using electrical parameters which separate pore throat from total porosity and effective from total hydraulic radius. The permeability of a pure shale is derived in a similar way but is strongly dependent on clay mineralogy. For the same porosity, there are 5 orders of magnitude of difference between the permeability of pure kaolinite and the permeability of pure smectite. The separate end-members' permeability models are combined by filling the sand pores progressively with shale and then dispersing the sand grains in shale. The permeability of sand shale mixtures is shown to have a minimum at the critical shale content at which shale just fills the sand pores. Pure shale has a slightly higher permeability. Permeability decreases sharply with shale content as the pores of a sand are filled. The permeability of sand shale mixtures thus has a very strong dependence on shale fraction, and available data confirm this distinctive shale-fraction dependence. In addition, there is agreement (within 1 order of magnitude) between the permeabilities predicted from our model and those measured over 11 orders of magnitude from literature sources. Finally, we apply our model to predict the permeabilities of shaly sand formations in the Gulf Coast. The predictions are compared to a data set of permeability determination made on side-wall cores. The agreement between the theoretical predictions and the experimental data is very good.

1. Introduction

Permeability is one of the most important and least predictable transport properties of natural materials. Permeability must be known to understand many natural phenomena including basin-scale hydrogeologic circulation [e.g., *Person et al*., 1996], fault dynamics [e.g., *Wintsch et al*., 1995], the safety of waste repositories [e.g., *Moore et al*., 1982], and many other problems related to subsurface hydrology. Many permeability models have been proposed [e.g., *Walsh and Brace*, 1984; *Bethke*, 1989; *Berryman*, 1992; *Nelson*, 1994]. These models generally relate permeability to geometric parameters of the porous media, particularly the hydraulic radius (the pore volume divided by the grain water interface area) and the porosity (which is sometimes corrected for bulk tortuosity). A recognized problem with these Kozeny-Carman (KC)-type relationships is that the porosity in sands and sandstones usually consists of large, isolated, roughly equidimensional voids which are connected by much smaller throats [*Krohn*, 1988; *Bernabé*, 1995]. The throats control the transport properties but contribute very little to the total porosity which is used in the permeability prediction. Recently, electrical parameters that separate pore throat from total porosity and effective from total hydraulic radius have been introduced to improve KC-type models [e.g., *Kostek et al*., 1992; *Bernabé*, 1995]. This paper presents a new model of permeability for sand shale mixtures based on these effective parameters. Clay type (illite, kaolinite, and smectite) is considered. The sand and shale end-members are combined using the geometric model of *Marion et al*. [1992]. The resulting permeability model for sand shale mixtures is shown to be compatible with available laboratory data and core measurements from the offshore Louisiana Gulf of Mexico and represents a significant improvement over the classical KC model.

2. Theory

2.1. Permeability of Clean Sand

The KC equation can be derived by considering a porous medium where the pores are cylindrical tubes of constant radius in the direction of flow. In such a case the filtration or Darcy velocity $\mathbf{J}_H$ is given by the Poiseuille's law [e.g., *Walsh and Brace*, 1984]:

$$\mathbf{J}_H = -\frac{R^2\phi}{8\eta_f}\nabla(p - \rho_f g z) \tag{1}$$

Here p is the fluid pressure, ρ_f is the density of the pore fluid, g is the gravity acceleration, z is the depth, R is the radius of the flow tubes, ϕ is the total porosity, and η_f is the dynamic shear viscosity of the fluid. The intrinsic permeability k is given by equating (1) to Darcy's law:

$$\mathbf{J}_H = -\frac{k}{\eta_f}\nabla(p - \rho_f g z) \tag{2}$$

[1]Now at Department of Geophysics, Centre Européen de Recherche et d'Enseignement de Géosciences de l'Environnement, Aix-en-Provence, France.

Paper number 98WR02700.
0043-1397/99/98WR-02700$09.00

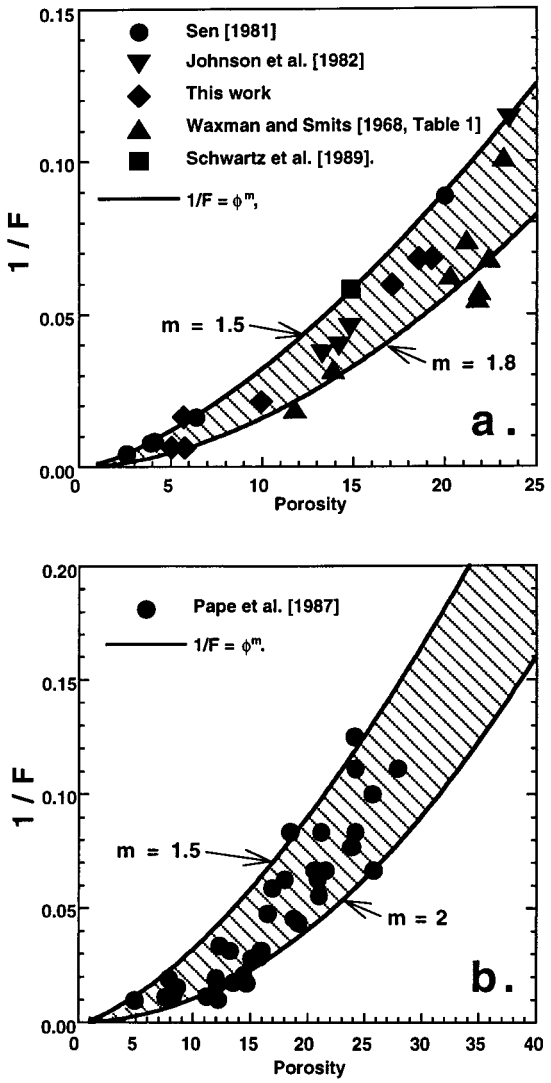

Figure 1. Inverse of the electrical formation factor versus the porosity (in percent). (a) Data from *Sen et al*. [1981], *Johnson et al*. [1982] (fused glass beads), and *Schwartz et al*. [1989] (numerical simulation on close-packed simple cubic array of insulating spheres in which the porosity decreases by uniform growth of the insulating phase in the pore space); others are clean natural sands and sandstones. (b) Data for clean and slightly shaly sandstones from *Pape et al*. [1987].

Noting that the ratio of pore volume to pore surface area, V_p/S, for this simple geometry equals $R/2$, the intrinsic permeability is

$$k = \frac{\phi}{2}\left(\frac{R}{2}\right)^2 = \frac{\phi}{2}\left(\frac{V_p}{S}\right)^2 \tag{3}$$

This is the original form of the KC equation, which is often generalized to $k = (V_p/S)^2\phi/(b\tau^2)$, where b is an empirical constant and τ^2 is the bulk tortuosity [*Walsh and Brace*, 1984]. For granular porous media with a unimodal grain size distribution the KC equation becomes $k = d^2\phi^3/[180(1 - \phi)^2]$, where d is the grain diameter (defined as the average value of the diameter of spheres of same volume than the grains). In (3) the permeability is related to two geometrical parameters, the porosity ϕ, and the hydraulic radius V_p/S. A major deficiency of the KC equation is that it does not distinguish effective from total properties. The fundamental postulate of *Johnson et al*. [1986] was that the KC equation could be improved by substituting electrical parameters for ϕ and V_p/S, where the electrical parameters were designed to capture the effective porosity and the effective hydraulic radius.

To understand how substituting electrical parameters might improved the KC equation, we consider how electrical current flows in an arbitrary porous medium with insulating minerals (the electrical flow is restricted to the interconnected pore space). In the absence of surface electrical conduction at the grain water interface the electrical current density in a representative elementary volume (REV), $\mathbf{J}$, is related to the macroscopic electrical field $\mathbf{E}$ (in V m^{-1}), by $\mathbf{J} = \sigma\mathbf{E}$. In such a case the relationship between the macroscopic electrical conductivity σ (in S m^{-1}) and the electrical conductivity of the fluid, σ_f (in S m^{-1}), is [e.g., *Revil and Glover*, 1997]

$$\sigma = \frac{\sigma_f}{F} \tag{4}$$

where F is a dimensionless, scale invariant parameter characterizing the pore space topology and called the electrical formation factor [*Johnson et al*., 1986]. The physical nature of the electrical formation factor can be understood if F is expressed as a normalized electrical field integral [*Avellaneda and Torquato*, 1991]:

$$\frac{1}{F} = \frac{1}{V}\int_{V_p} |\mathbf{e}_b|^2\, dV_p \tag{5}$$

where $\mathbf{e}_b \equiv -\nabla\psi/|\mathbf{E}|$ is the normalized electrical field in the interconnected pore space, $|\langle \mathbf{e}_b \rangle| = 1$, where $\langle\ \rangle$ is the volume-averaging operator, $\nabla\psi$, the local electrical potential gradient in the pore space, is analogous to the local fluid pressure gradient, V is the volume of the REV, and V_p is the interconnected pore volume. The distribution $|\mathbf{e}_b|^2$ acts as a weighting function for the total interconnected porosity $\phi = V_p/V$. It gives less weight to pores which transmit little current (e.g., $|\mathbf{e}_b|^2$ vanishes in dead ends as a consequence of the conservation of electrical charges). The electrical potential gradients are concentrated in the throats of the interconnected pore space, and therefore the throats contribute the most to $1/F$. Consequently, the inverse of the formation factor, $1/F$, in (5) is a useful measure of the effective interconnected porosity. The electrical formation factor is related to the porosity by the empirical Archie relationship [*Waxman and Smits*, 1968]:

$$F = \phi^{-m} \tag{6}$$

where m is the so-called "cementation exponent" and varies with the pore geometry inside a range 1–4. *Sen et al*. [1981] show that in the case of granular porous media, (6) can be derived from first principles (actually, the charge conservation equation). They calculated a theoretical value of $m = 1.5$ using a differential effective medium approach for an assemblage of perfect spherical grains. Figure 1 shows that the cementation exponent of fused glass beads and sands and sandstones with a wide range of porosities (0.03–0.30) lies between 1.5 and 2.0 ($m > 1.5$ probably because the grains are not perfectly spherical). If the interconnected pore space consists entirely of interconnected open cracks and fractures so that most of the porosity conducts electrical current, $m \approx 1.1$–1.3. By contrast, a high cementation exponent ($m > 2.5$) results if large pores are connected by narrow throats. For example, the

cementation exponent of an artificial porous medium with big spherical pores interconnected by narrow throats called Syporex® (porosity of 79.7%) is 3.8 ± 0.1 (Figure 2 and Table 1). Such a high value indicates a strong decoupling between the total interconnected porosity and the effective porosity that controls flow.

An effective electrical pore radius Λ can be defined if the grains are coated with a thin layer where electrical conductivity differs from that of the pore fluid [*Johnson et al*., 1986]. This thin layer represents the electrical double layer. By equating the macroscopic Joule dissipation to the sum of the electrical Joule dissipations in the pore space, *Johnson et al*. [1986] showed that the macroscopic electrical conductivity in a REV is given at high salinities by

$$\sigma = \frac{1}{F}\left(\sigma_f + \frac{2}{\Lambda}\Sigma_S\right) \tag{7}$$

where Σ_S and Λ are defined by

$$\Sigma_S = \int_0^{\chi_D} [\sigma(\chi) - \sigma_f]\, d\chi \tag{8}$$

$$\frac{2}{\Lambda} = \frac{\int_S |\mathbf{e}_b|^2\, dS}{\int_S |\mathbf{e}_b|^2\, dV_p} \tag{9}$$

where $\mathbf{e}_b$ is the same local normalized electric field as that used to define F in (5) [*Johnson et al*., 1986], χ is the local distance perpendicular to the pore grain interface, $\sigma(\chi)$ is the local conductivity in the vicinity of the grain surface, χ_D is the thickness of the electrical double layer, Σ_S is called the specific surface conductance and represents the "anomalous" conduction in the electrical double layer [*Revil and Glover*, 1997, 1998]. The length scale Λ represents a weighted analog of the length $2V_p/S$ exactly in the same sense that $1/F$ represents a weighted analog of the porosity. Both use the same electrical weighting function. Consequently, we can replace V_p/S by Λ and ϕ by $1/F$ in the KC equation, equation (3), with the result that

$$k = \frac{\Lambda^2}{2F} \tag{10}$$

Using numerical simulations, *Kostek et al*. [1992] have shown that (10) provides a very good approximation to the intrinsic permeability. Equation (10) is valid in principle for a very wide range of porous media, but *Bernabé and Revil* [1995] have noted that Λ is not easy to determine from electrical conductivity measurements. In Appendix A we establish a new relationship between Λ, the cementation exponent, and the radius of the grains

$$\Lambda = \frac{R}{m(F-1)} \approx \frac{R}{mF} \tag{11}$$

If we take $m^2 \approx 3$ as an average value for sands and sandstones (see Figure 1 where $1.5 \leq m \leq 2$ for clean sands) in (11) and substitute (11) into (10), we obtain a new equation for the permeability (in m^2) of a clean sand or sandstone of porosity ϕ_{Sd} (fraction):

$$k_{Sd} = \frac{R^2}{2m_{Sd}^2 F^3} = \frac{d^2(\phi_{Sd})^{3m_{Sd}}}{24}, \tag{12}$$

where $d = 2R$ is the grain diameter (in m) and m_{Sd} is the cementation exponent for clean sands and sandstones, and we have used Archie's law, equation (6), to obtain the right-hand side expression.

Figure 3 tests (12) for randomly packed grains with a porosity in the range 0.38–0.42. Equation (12) is also tested in Figures 4 and 5. In Figure 5a, (12) is compared with a large data set of permeability measurements on similar grain size sediments of different porosity from *Chilindar* [1964, Figure 2, p. 73]. In Figure 5b, (12) is compared with the prediction of the KC equation. Our model is clearly able to predict the permeability of granular porous media much better than the KC equation which can overestimate the permeability of more than 2 orders of magnitude at permeability ~1 mD. For natural sandstones the electrical conductivity data of *Waxman and Smits* [1968] lead to a cementation exponent: $m \approx 1.82 \pm 0.08$ for 20 clean sandstone samples. Taking $m = 1.8$ as an average value, our relationship becomes $k = d^2\phi^{5.1}/24$. This equation has a form similar to an empirical formula *Berg* [1975] suggested for sandstones: $k = 8.4 \times 10^{-2}\, d^2\phi^{5.1}$ (k is in m^2; d is in m; and ϕ is a fraction).

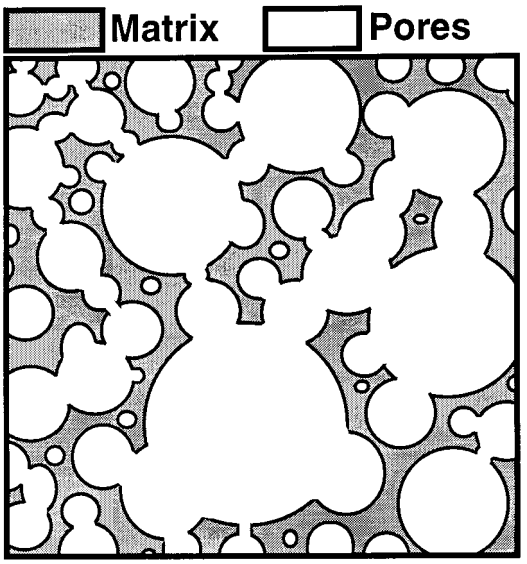

Figure 2. Microstructure of Syporex®. Syporex® shows two types of pores: large, isolated, roughly equidimensional voids and much smaller throats. The throats control the transport properties but contribute very little to the porosity. Consequently, the porosity and the inverse of the electrical formation factor, which represents the effective porosity of the pores controlling transport properties in the interconnected pore space, should have very different values. This is confirmed by the high value of the cementation exponent measured for three Syporex® samples.

Table 1. Formation Factor and Cementation Exponent of Syporex®

Sample	Porosity	F	m
SI	0.7955	2.36	3.75
SII	0.7968	2.43	3.91
SIII	0.7969	2.29	3.65

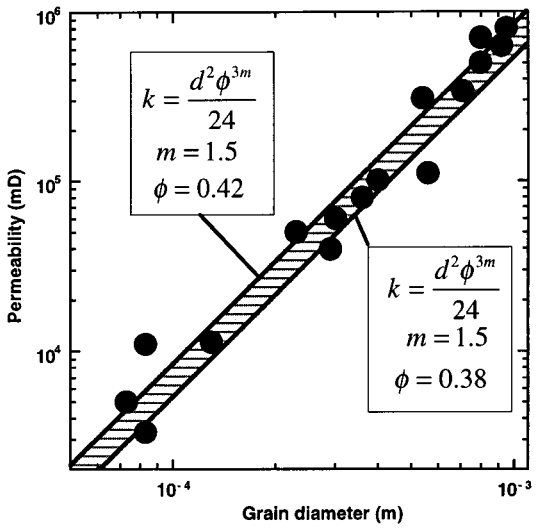

Figure 3. Variation of permeability with grain diameter (1 mD $\approx 10^{-15}$ m^2) (experimental data reported by *Bear* [1988]).

2.2. Permeability of Shale

When investigating the permeability of shale, it is very important to consider only permeability measurements that have been made with saline water. This is because fresh water destabilizes clay minerals, and the permeabilities measured with fresh water are greatly underestimated [*Moore et al*., 1982]. At high salinities, cations from the electrolyte are directly adsorbed in the Stern layer, and this adsorption stabilizes the clay mineral surface [*Rowlands et al*., 1997]. Low-salinity or distilled water reduces the capacity of the Stern layer to stabilize clay particles with the result that clay particles detach, float into the pore space, plug the pore throats, and block flow. Laboratory experiments suggest that increasing electrolyte into a compacted shale may result in greater permeability of the shale to the electrolyte [*Von Engelhardt and Gaida*, 1963; *Mesri and Olson*, 1971; *Whitworth and Fritz*, 1994]. The permeability of natural shale measured with 0.2 *N* NaCl solution is always higher than 1×10^{-6} mD (1 mD $\approx 10^{-15}$ m^2) [*Gondouin and Scala*, 1958], whereas the permeability measured with pure water can reach values as low as 1×10^{-8} mD [*Dickey*, 1970].

For shale, (12) remains valid with k_{Sh}, m_{Sh}, and ϕ_{Sh} replacing k_{Sd}, m_{Sd}, and ϕ_{Sd}, respectively. What is the cementation exponent for shales? The measured cementation exponent of shale or very shaly sand appears to be much larger ($m \sim 2$–4) than the cementation exponent associated with clean sands ($m \sim 1.5$–2) [*Waxman and Smits*, 1968]. According to our model, this suggests that the permeability of a shale should be much more strongly dependent on porosity than the permeability of a sand. This is confirmed by *England et al*. [1987], who used a relationship between permeability and porosity for shales and mudstones given by $k = 4 \times 10^{-15}\ \phi^8$ (in m^2). Using (12) leads to a cementation exponent $m_{Sh} = 2.7$ in agreement with the range of values reported by *Waxman and Smits* [1968]. *Mendelson and Cohen* [1982] generalized the electrical conductivity model of *Sen et al*. [1981] (valid for spherical grains) to ellipsoidal grains with arbitrary distributions of orientation and depolarizing factors. Highly oblate (i.e., disk-shaped) ellipsoidal grains with grain eccentricity of ~4 raises m to values close to the maximum observed value of 4 observed in Figure 6.

The permeability of pure clays has been measured by *Mesri and Olson* [1971, Figure 6, p. 156]. The measurements were made with saline pore fluids and are probably among the best available. Their data indicate that the permeabilities of kaolinite, illite, and smectite at a porosity of 0.50 and a salinity of 1–0.1 *N* ($CaCl_2$ and NaCl) are 0.10, 5×10^{-4}, and 1×10^{-6} mD, respectively. These permeabilities are not surprising because the specific surface area (which is inversely proportional to the grain radius) is larger for smectite (700–900 m^2 g^{-1}) than for illite (~80–100 m^2 g^{-1}) and kaolinite (10–20 m^2 g^{-1}) [*Patchett*, 1975]. In Figure 6 we analyze the dependence of the *Mesri and Olson* [1971] permeability measurements on porosity reduced by compaction. The relative reduction of the grain diameter during mechanical compaction is much smaller than the relative reduction of porosity (A. Revil et al., in preparation, 1998). Consequently, permeability variations with the ef-

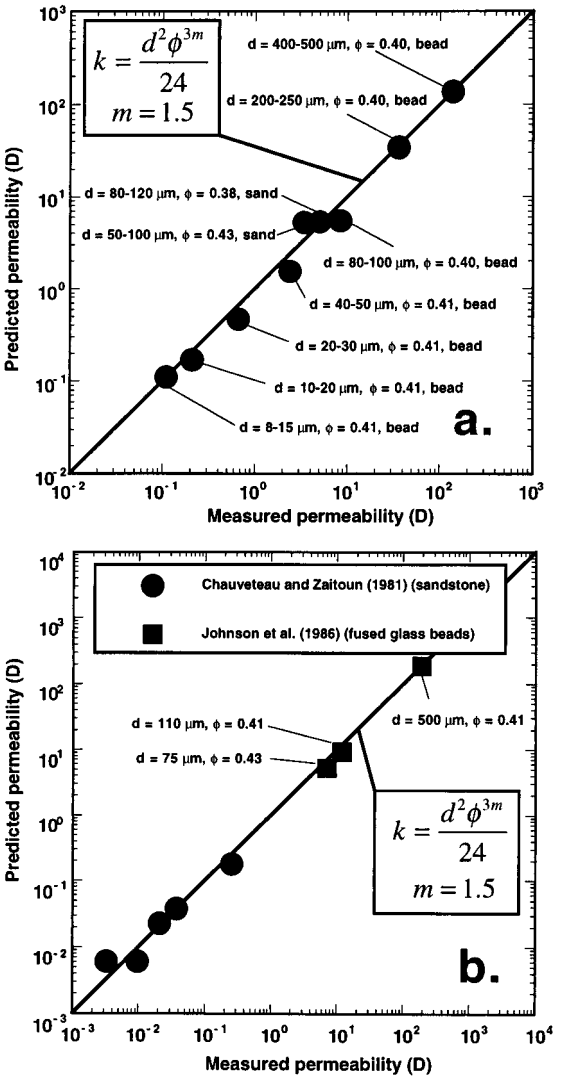

Figure 4. Permeability for granular porous media. (a) The data are from *Chauveteau and Zaitoun* [1981] for unconsolidated sand and beads. (b) The data are from *Chauveteau and Zaitoun* [1981] for natural sandstone (we have assumed a grain diameter of 250 μm for the calculation) and *Johnson et al*. [1986] for fused glass beads.

fective stress during compaction results mainly from porosity variations. From (12) the shale end-member permeability k_{Sh} is related to the shale end-member porosity ϕ_{Sh} by

$$k_{Sh} = k_0(\phi_{Sh}/\phi_0)^{3m_{Sh}} \tag{13}$$

where k_0 and ϕ_0 are the permeability and porosity in a reference state, respectively (we take $\phi_0 = 0.50$). Using (13) and the permeability porosity data reported in Figure 6, we calculate m and k_0 for each end-member clay mineralogy (kaolinite, illite, and smectite), and we report them in Table 2. The cementation exponent range observed from this permeability analysis is in agreement with the values of m_{Sh} cited previously and with those resulting from electrical conductivity measurements [e.g., *Mendelson and Cohen*, 1982]. The important point of Figure 6 is that it shows the porosity dependence of permeability of pure clays is predicted well by (13).

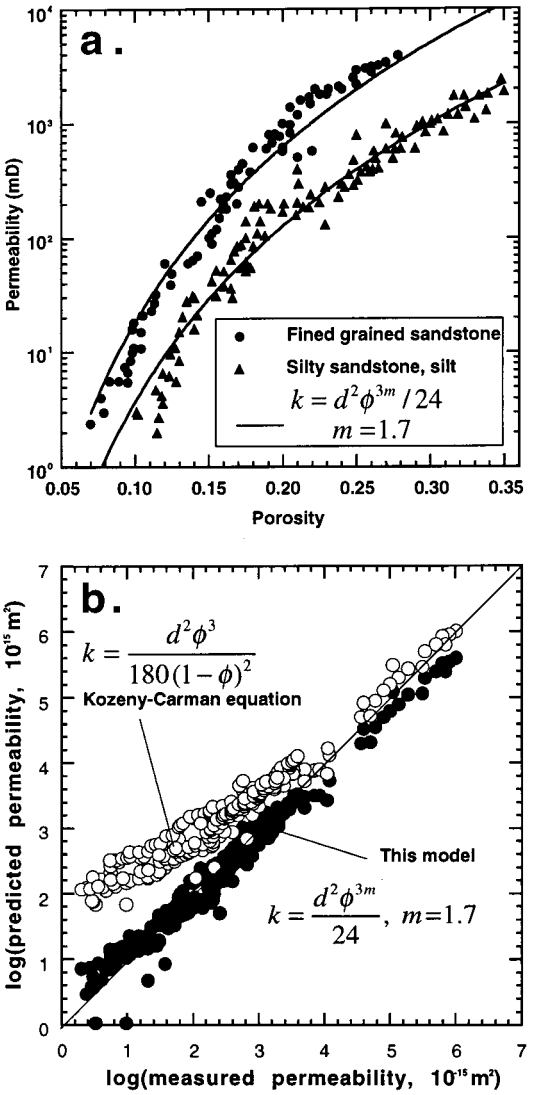

Figure 5. Test of the model developed in that main text. Figure 5a shows the relationship between porosity and permeability of fine-grained and silty sandstones (data from *Chilindar* [1964, Figure 2, p. 73]). The average grain diameter derived from this model by fixing $m = 1.7$ and using a regression analysis on the data of Chilindar is 235 μm for the fine-grained sandstone and 103 μm for the silty sandstone in agreement with the observations. Figure 5b shows the comparison between the predictions of the Kozeny-Carman model and the present model (all the data from Figures 3, 4, and 5a are used).

Table 2. Permeability Porosity Relationship for Shales

Shale	m	$k_0(\phi_0 = 0.50)$, mD
Kaolinite	2.34–3.15	7.1–0.10
Illite	3.28	5.1×10^{-4}
Smectite	4.17	3.1×10^{-7}

Where $k = k_0(\phi/\phi_0)^{3m}$.

2.3. Porosity and Permeability of Sand Shale Mixture

In sand-shale mixtures, porosity is not a simple function of the shale fraction. Porosities of pure sand and shale are higher than the porosity of a sand shale mixture. Porosity is reduced as clay fills the pores of a sand or as sand is dispersed in a shale. For mixtures of sands and shales the porosity is given by *Marion et al*. [1992]:

$$\phi = \phi_{Sd} - \varphi_V(1 - \phi_{Sh}) \qquad \varphi_V \le \phi_{Sd} \tag{14}$$

$$\phi = \varphi_V\phi_{Sh} \qquad \varphi_V \ge \phi_{Sd} \tag{15}$$

where φ_V is the clay volume fraction and ϕ_{Sd} and ϕ_{Sh} are the porosity of the clean sand and pure shale end-members, respectively (Figure 7). A sediment with a shale content which ranges from $\varphi_V = 0$ to that which just fills all the sand pores ($\varphi_V = \phi_{Sd}$) is called a "clayey sand." A sediment with a greater shale content than this ($\varphi_V > \phi_{Sd}$) is called a "sandy shale." The porosity of sand shale mixture has a minimum at the clayey sand-sandy shale boundary given by $\phi = \phi_{Sd}\phi_{Sh}$. *Koltermann and Gorelick* [1995] show that (14) and (15) are good first-order approximations to the porosity of a binary mixture assuming ideal packing (see *Koltermann and Gorelick* [1995] for nonideal packing). Ideal packing is a good approximation when the ratio between the coarsest and the finest grain size is large. This is the case for sand shale mixtures where sand grain diameters are larger than 50 μm and clay grain diameters are smaller than 5 μm. For practical reasons such as downhole measurements analysis it is very useful to have relationships between the shale fractions in volume and weight which are provided in Appendix B.

In the clayey sand domain we expect, from (12), that the permeability of a clayey sand ($k\phi$) is related to the permeability of a clean sand ($k_{Sd}\phi_{Sd}$):

$$k = k_{Sd}\left(\frac{\phi}{\phi_{Sd}}\right)^{3m_{cs}} \tag{16}$$

where m_{cs} is the cementation exponent corresponding to the clayey sand domain. Because clays in the pore throats block flow, m_{cs} should depend strongly on the shale content, particularly near the boundary between the clayey sand and sandy shale domains. Because the flow blockage is severe near this boundary, we intuitively expect than m_{cs} is not only a positive function of the shale content but can reach values much higher than 2. Following the above logic, we expand m_{cs} as a power function of φ_V:

$$m_{cs} = m_{cs}^0 + m_{cs}^1\varphi_V + O(\varphi_V^2) \tag{17}$$

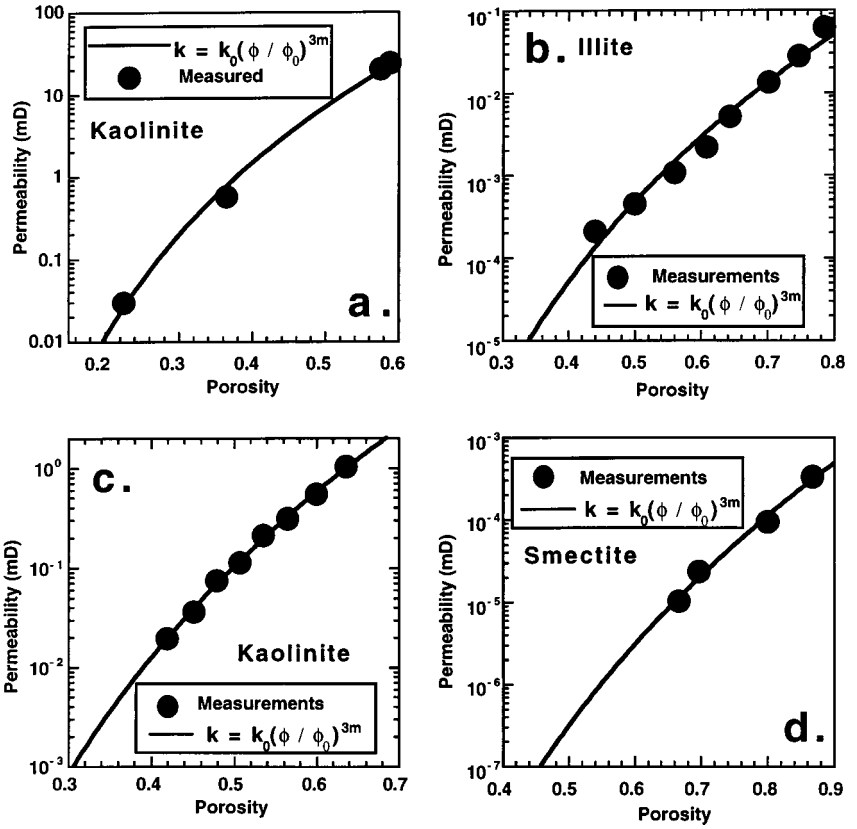

Figure 6. Permeability/porosity relationship for kaolinite, illite, and smectite: (a) data from *Olsen* [1966], (b) data from *Mesri and Olson* [1971], 1 *N* NaCl, (c) data from *Mesri and Olson* [1971], 1 *N* NaCl, and (d) data from *Mesri and Olson* [1971], 0.1 *N* NaCl.

where $m^0_{cs} = m_{Sd}$ is the cementation exponent of the clean sand and is in the range 1.5–2.0 (Figure 1). Combining (14) and (16), we have in the clayey sand domain:

$$k = k_{Sd}\left[1 - \varphi_V\left(\frac{1-\phi_{Sh}}{\phi_{Sd}}\right)\right]^{3m_{cs}} \qquad \varphi_V < \phi_{Sd} \qquad (18)$$

At the clayey sand-sandy shale boundary, $\varphi_V = \phi_{Sd}$, we have

$$k = k_{Sd}(\phi_{Sh})^{3m_{cs}} \qquad \varphi_V = \phi_{Sd} \qquad (19)$$

where $m_{cs} = m^0_{cs} + m^1_{cs}\phi_{Sd}$. We present arguments in Appendix C that the permeability in the sandy shale domain can be adequately represented by

$$k = \frac{k_{Sh}}{F_{Sd}} \qquad \varphi_V > \phi_{Sd} \qquad (20)$$

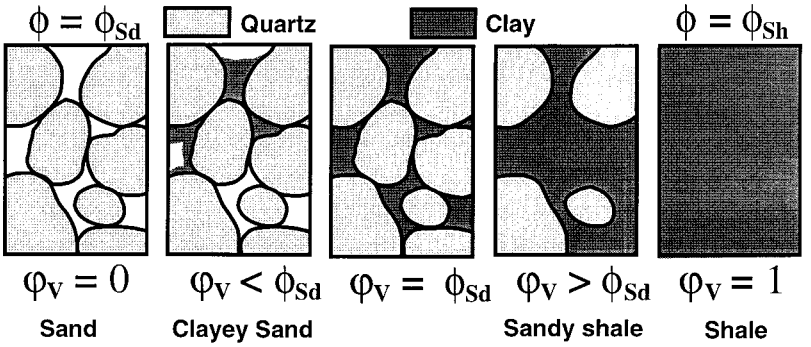

Figure 7. Sand shale mixture for various shale contents. The shale content increases from the left to the right. For a clay-free sand (first end-member), the noncompacted porosity is equal to ϕ_{Sd}. For a clayey sand the porosity decreases because of the presence of clay particles in the pore space. This decrease continues until the critical point where all the pore space of a clean sand is occupied by clay particles, i.e., when the shale content is equal to the porosity of a clean sand. After this point the rock is a sandy shale, and an increase in shale content is only possible through replacement of quartz grains by clay particles, and the porosity increases with the shale content. The second end-member is a pure shale with no quartz grains and with a porosity equal to ϕ_{Sh}.

Equation (20) suggests that sandy shale permeability can be obtained by taking into account the flow blockage by the sand grains. The parameter F_{Sd} is the formation factor for the sand grain skeleton (Figure 8). Using Archie's law, $1/F_{Sd} = (\varphi_V)^{m_{Sd}}$, and (20), the permeability in the sandy shale domain is given by

$$k = k_{Sh}(\varphi_V)^{m_{Sd}} \qquad \varphi_V > \phi_{Sd} \tag{21}$$

Since permeability must be continuous across the clayey sand-sandy shale boundary, (19) must equal (21) at this boundary. The important result is that k_{Sh} can be determined by extrapolating permeabilities in the sandy shale domain to the known clayey sand boundary:

$$k_{Sh}(\phi_{Sd})^{m_{Sd}} = k_{Sd}(\phi_{Sh})^{3m_{Sd}+3m^1_{cs}\phi_{Sd}} \qquad \varphi_V = \phi_{Sd} \tag{22}$$

Equation (22) can be also used to determine m^1_{cs} from the permeability and porosity of the two end-members.

Equations (12), (17), (18), (21), and (23) represent a new model for the permeability of sand shale mixtures which describes permeability from clean sand ($\varphi_V = 0$) to pure shale ($\varphi_V = 1$). These permeability functions are plotted from different grain sizes as a function of shale content in Figure 9a. An important conclusion from Figure 9a is that the permeability of a sand shale mixture increases with increasing shale content past the clayey sand-sandy shale boundary because sand grains (with no intrinsic permeability) are replaced by shale (which has a permeability). The minimum permeability occurs at $\varphi_V = \phi_{Sd}$. In Figure 9b the permeability of sand shale mixtures is plotted as a function of porosity. The permeability variations in Figure 9b result only from shale content variations. There is no compaction contrary to Figure 5a.

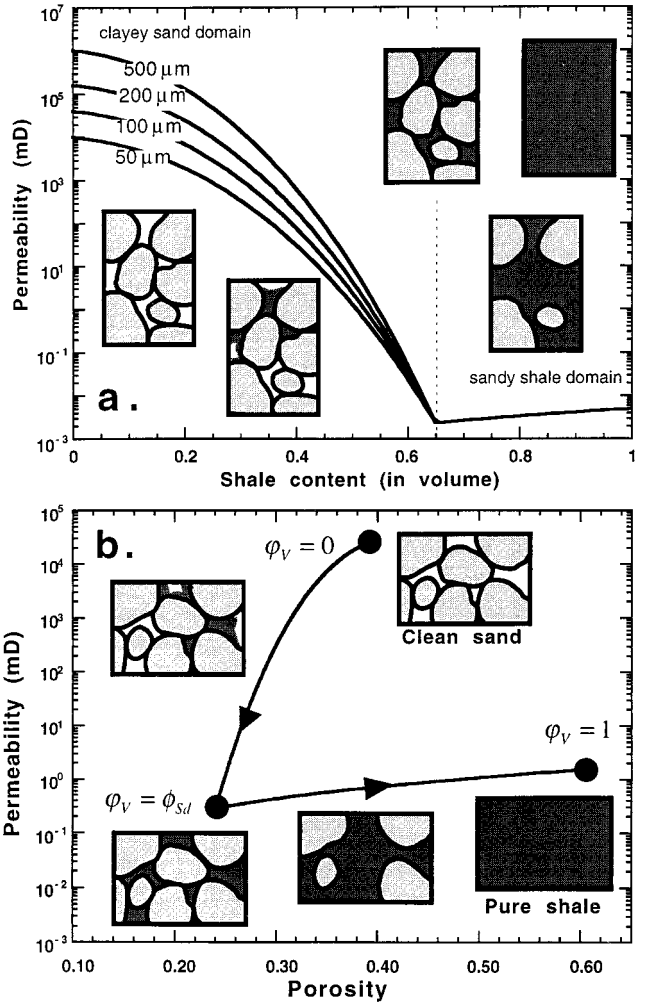

Figure 9. Permeability of sand shale mixtures. Figure 9a shows the permeability versus sand content (in volume). The permeability is plotted as a function of the shale content for four grain sizes of the sand (500, 200, 100, and 50 μm). There is a minimum in the permeability which corresponds to the limit between the clayey sand and sandy shale domains. The parameters used are $\phi_{Sd} = \phi_{Sh} = 0.65$, $k_{Sh} = 5 \times 10^{-3}$ mD, and $m_{Sd} = 1.80$. Figure 9b shows the permeability versus porosity for sand shale mixtures. The arrows correspond to an increase of the shale content from $\varphi_V = 0$ (clean sand), $\varphi_V = \phi_{Sd}$ (the sand is filled with clays), and $\varphi_V = 1$ (pure shale).

3. Application

3.1. Evaluation by Comparison to Laboratory Data

Our permeability model is compared to experimental data in Figure 10. As shale content increases from 0 to $\varphi_V = \phi_{Sd} = 0.40$, permeability decreases sharply from 2.7×10^4 to 5.3×10^{-1} mD. Adding a small amount of clay to a clean sand has a dramatic effect on the permeability. As shale content increases from 0.40 to 1, permeability increases slightly to 1.5 mD. The agreement between the model and data is very good. An important point in Figure 10 is that it directly confirms that permeability increases with shale content past the clayey sand-sandy shale boundary and that permeability has a minimum when plotted as a function of the shale fraction. These are critical predictions of our model.

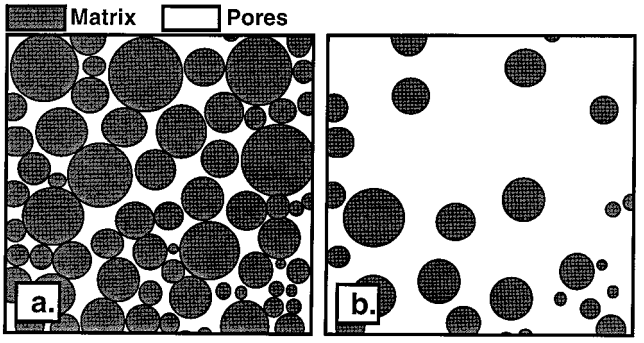

Figure 8. Sand grain skeleton in the sandy shale domain. The sand grain skeleton is obtained by replacing the clay particles by pore space in order to evaluate the electrical formation factor associated with the sand grains. (a) At the clayey sand-sandy shale limit the electrical formation factor of the sand grain skeleton is equal to the electrical formation factor of a clean sandstone. (b) In the limit of a shale the sand grain skeleton is equivalent to a dilute suspension of spherical particles, and its associated electrical formation factor is given by the Hashin-Shtrikman lower bound.

3.2. Evaluation by Comparison to Field Data

In sedimentary basins, detrital sand grains and clays are mixed in a broad range of sand shale ratios [*Matlack et al.*, 1988]. This is the case, for example, in the Gulf Coast [*Holland*, 1990]. We compare permeabilities predicted by our model to a very large data set of permeabilities determined on side-wall cores from the South Eugene Island (SEI) salt withdrawal

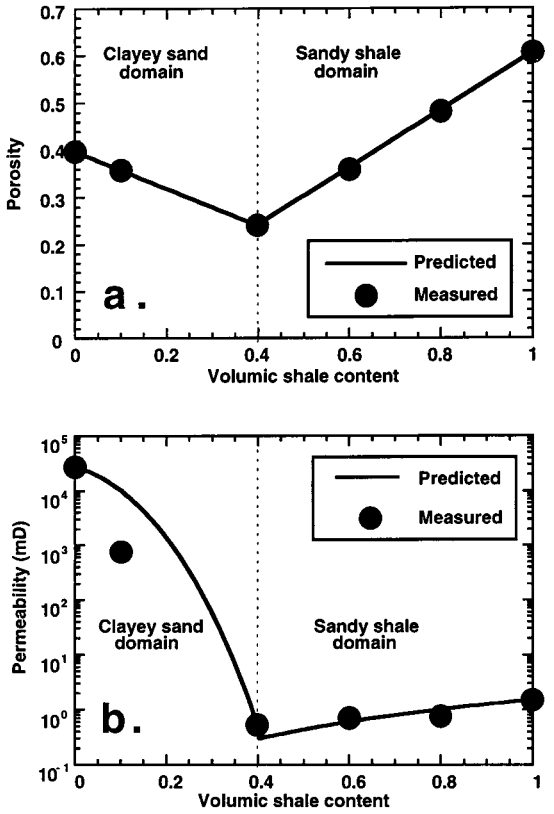

Figure 10. Porosity and permeability versus clay content (in volume). (Experimental data are from *Knoll and Knight* [1994]; the clay is kaolinite.) Parameters used are $\phi_{Sd} = 0.40$, $\phi_{Sh} = 0.60$, $k_{Sd} = 27 \times 10^3$ mD, and $k_{Sh} = 1.50$ mD; grain densities are 2650 kg m^{-3}.

minibasin. This minibasin is a young Pleistocene passive shelf-margin sedimentary basin located in the Gulf of Mexico offshore Louisiana. During the last 2.8 Ma a thick sequence of shale was deposited over pre-Tertiary sediments and covered by increasingly sand-rich sediments [*Holland et al.*, 1990]. Gamma ray and density logs from a borehole in the SEI minibasin are used to calculate porosity and shale content as a function of the depth (Figure 11, the method is reported by *Revil et al.* [1998a]). The section is composed of sandy shale with several massive sandy units. No clean sand unit is observed in this area, and all the sandy layers are sand shale mixtures [*Holland et al.*, 1990].

We select data from two sandy units: the GA sand at 1450 m depth and the HB sand at 1650 m depth. The diameters of the grains in the GA and HB sand layers are in the range 80–190 and 50–250 μm, respectively. The detrital clay fraction in GA and HB sands occurs mainly as pore-filling cement. Thin sections we have analyzed indicate that the clay mineralogy is fairly constant over the depth intervals selected. The depositional environment corresponds to a fluvial zone (between the surface and ~1500 m depth) and a proximal deltaic zone (~1500–2500 m). The clay mineralogy is mixed layer illite/smectite clays (ML), 64.5%; kaolinite (K), 15.5%; chlorite (C), 18.25%; and illite (I), 1.75%. The pore fluid overpressure is very small in both GA and HB units. Consequently, we consider these units as hydrostatically pressured.

Laboratory determination of core permeability are representative of the in situ permeabilities despite the fact that the cores have decompressed when they were taken from ~1.5 km depth to the surface. The reason is that the change in porosity associated with this decompression is very small (<3%). To compare these permeabilities to the predictions of our model, however, we need to compact the sand and shale components of our model to the porosities of clean sand and pure shale at the depths corresponding to the occurrence of the GA and HB units. The relationship between the in situ porosity ϕ and the uncompacted porosity ϕ_0 is given by [*Revil et al.*, 1998b]:

$$\phi = 1 - (1 - \phi_0) \exp(z/z_c) \tag{23}$$

where z is the depth, $1/z_c \equiv g(\rho_g - \rho_f)\phi_0\beta$, β is the compaction coefficient ($\beta = (3.3 \pm 0.3) \times 10^{-8}$ Pa^{-1} in the SEI minibasin), and ϕ_0 is the uncompacted porosity. The uncompacted porosity of pure shale in Eugene Island is 0.65. Using $z = 1450$ m for the GA unit and $z = 1650$ m for the HB unit, we obtain $\phi_{Sh} = 0.44$ and 0.40 in the GA and HB units, respectively. The porosity of a clean sand at these depths is taken to be equal to 0.40, i.e., the porosity of a random assemblage of spheres. We do not compact the sand porosity below this random packing limit because we see no evidence of significant sand grain pressure solution in core thin sections.

We first plot the permeability versus porosity for the samples

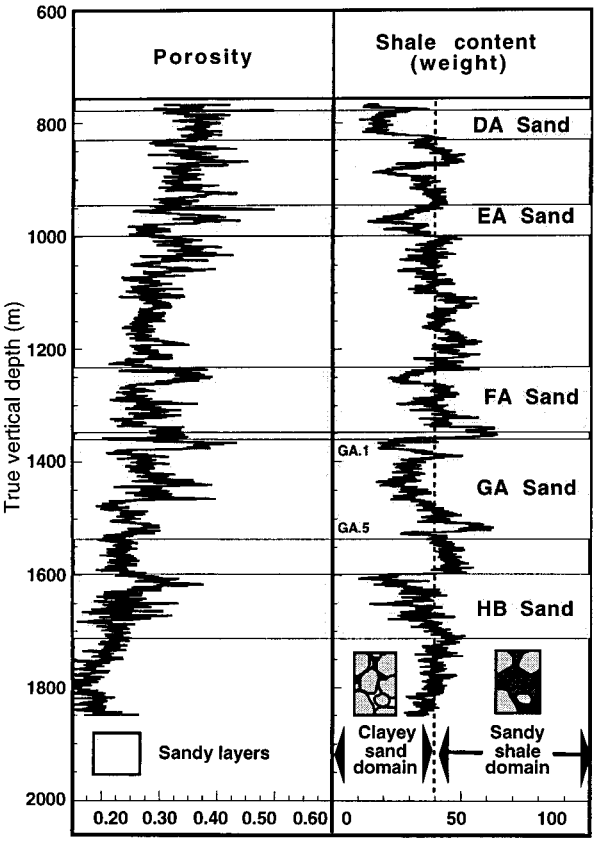

Figure 11. Hydrostatic porosity analysis. Porosity profiles result from a combination of a large-scale trend of decrease of the porosity with depth which reflects mechanical and chemical compaction and high-frequency porosity variations resulting from sand/shale ratio variations with depth. Below a shale fraction by weight of 0.39 the sand shale mixture is shown theoretically to be a clayey sand whereas up to this limit the mixture is a sandy shale. This is furthermore checked in the present case by coring.

from each sandy layer (Figure 12). The state of compaction is identical for all the samples from the same unit, and the porosity variations result only from shale content variations. We use Figure 12 to discriminate between clayey sands and sandy shales by assuming, as in Figure 9b, the kick in the trajectory occurs at the critical shale content. Then we convert porosity to shale content using (14) and (15). Permeability as a function of the shale content is shown in Figure 13. The determined values compare very well with the predictions of our model which allow us to determine the permeability of clean sand (at $\varphi_V = 0$), the permeability of pure shale ($\varphi_V = 1$), and the minimum permeability of the formations (at $\varphi_V = \phi_{Sd}$). The results are reported in Table 3. The grain sizes resulting from the extrapolated permeability of a clean sand in Figure 13 and the application of (12) are given in Table 3. They are compatible with the observations reported by *Holland et al.* [1990]. We can also determine the value of the cementation exponent at the boundary between the clayey sand domain and the shaly sand domain, i.e., at $\varphi_V = \phi_{Sd}$. At this boundary the cementation exponent of the sand/shale mixture should be equal to the cementation exponent of a pure shale, i.e., in the range 2–4. Taking (17) with $\varphi_V = \phi_{Sd}$, we have $m = m_{Sd} + m^1_{cs}\phi_{Sd}$. From the permeability data analyzed previously we have $m^1_{cs} = 5.08$ and 3.54 for the GA and HB units, respectively. Taking $m_{Sd} = 1.8$ (Figure 1) and $\phi_{Sd} = 0.40$, m at $\varphi_V = \phi_{Sd}$ equals 3.83 and 3.22 for the GA and HB units, respectively. These values are in agreement with the values in Table 2 and also in agreement with the upper values of $m = 4$ reported by *Mendelson and Cohen* [1982].

The shale permeability is approximately in the range 2–4 mD, and the minimum permeability is in the range 0.4–0.7

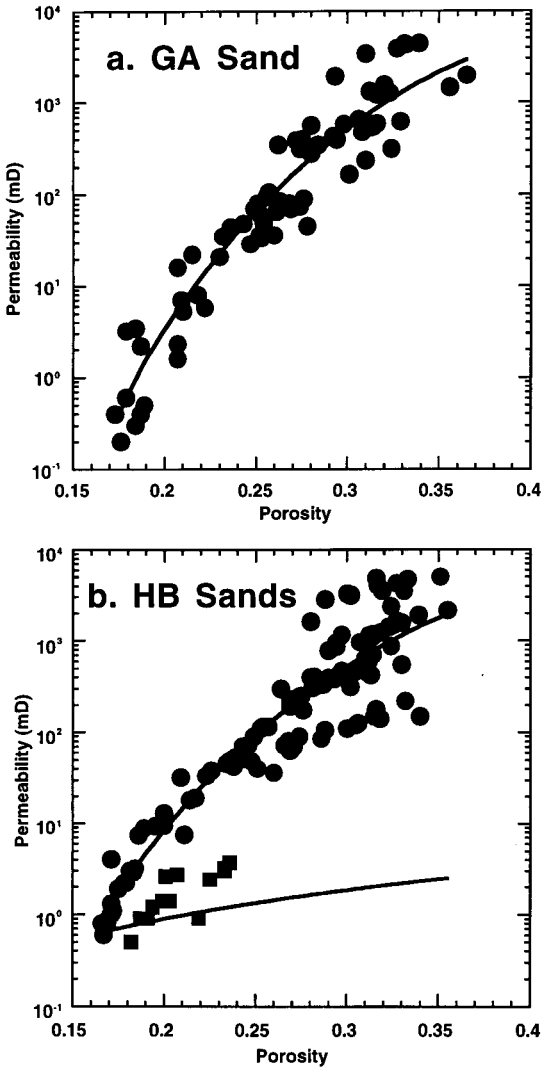

Figure 12. Permeability versus porosity (GA and HB sands). Figure 12a shows cores from the GA sand unit. The plot of the permeability versus porosity for the data set from the GA sand unit indicates clearly that these cores are clayey sands. Figure 12b shows cores from the HB sand units. Two subgroups can be separated from the permeability/porosity analysis: clayey sand and sandy shale.

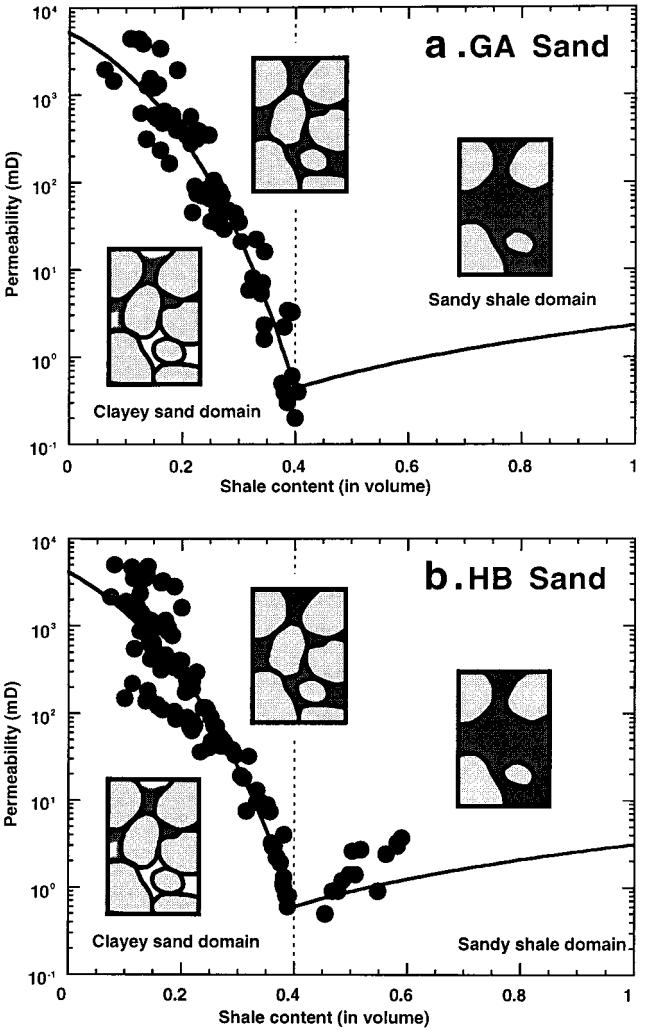

Figure 13. Permeability versus shale content (in volume) for GA and HB sands.

Table 3. Results From the Permeability Analysis

Sedimentary Layer	Sand Grain Diameter, μm	Shale Permeability, 10^{-15} m^2	Minimum Permeability, 10^{-15} m^2
GA	132	2.27	0.44
HB	118	3.54	0.68

mD. These values agree with initial in situ permeability measurements made on the Pathfinder well when fluid was first introduced into the well under close to in situ pressure conditions. The Pathfinder well was drilled in 1993 as a part of a Global Basins Research Network/Department of Energy/oil industry cost sharing project into a major fault of SEI minibasin. The early drill stem tests which injected fluids at slightly overpressure indicate a minimum stable permeability slightly less than 0.1 mD in agreement with the previous data. The high permeability of the shale fraction in the sedimentary section analyzed above and measured in the field probably results from the size of the clay crystals. The clay fraction contains mainly recrystallized illite and mixed layer clay. The cation-exchange-capacity (CEC) of clays represents the charge deficit of the clays per unit mass of grains, and it is proportional to the specific surface area [*Patchett*, 1975], which is inversely proportional to the grain diameter. The CEC of the shale fraction from the SEI minibasin is very close to the CEC of pure kaolinite. Consequently, the average grain diameter of the shale fraction in the SEI minibasin is probably equal to the grain diameter of kaolinite which explains the relatively high permeability of the shale fraction. Taking (13) with $k_0 = 7$ mD at $\phi_0 = 0.50$ (see Figure 6a for kaolinite) and $m = 3$, we obtain a permeability for the shale fraction equaling 1 mD at $\phi = 0.40$ in agreement with the shale permeability obtained from our permeability model (Table 3).

4. Discussion and Conclusions

The conclusions reached in this paper are the following: (1) the classical Kozeny-Carman relationship is improved by using electrical parameters which separate pore throat from total porosity and hydraulic radius. We develop a model for the permeability of a clean sand as a function of the grain diameter, the porosity, and the electrical cementation exponent. The model predicts the permeability of clean sands inside 1 order of magnitude to over more than 6 orders of magnitudes. (2) The permeability of a pure shale is derived in a similar way but is strongly dependent on clay mineralogy. (3) We derive a permeability model able to predict the permeability of sand shale mixtures as a function of shale fraction and the permeability of the two end-members (clean sand and pure shale). The permeability of sand shale mixtures is shown to have a minimum at the critical shale content at which shale just fills the sand pores, and pure shale has a slightly higher permeability. Permeability decreases sharply with shale content as the pores of a sand are filled. These critical predictions of the model agree with experimental data sets within 1 order of magnitude over 11 orders of magnitude. (4) An application of the permeability model to Gulf Coast side-wall cores data suggests that our model predict very well the permeabilities of natural shaly sand formations.

Two questions are now discussed. What is the implication of our model for the understanding of the permeability of clay-bearing sands and sandstones?, and what is the particular value of the model in the area of water resources? As it has been demonstrated in this paper, the permeability model requires only accessible parameters: (1) the grain size distribution of the sand fraction, (2) the clay mineralogy, (3) and the shale content (either in volume or in weight). In addition to these parameters, we need to consider the state of compaction of the two end-members (clean sand and perfect shale). This model should only be considered as a first step in order to derive a rigorous model addressing the field permeability of sand shale mixtures. This is because the permeability of clay-bearing sands is not simply related to the permeability of the two end-members but may be influenced by depositional and diagenetic processes influencing their present pore structure (J. P. Raffensperger, personal communication, 1998). For example, transport, dissolution, dispersion, and flocculation of clays would have a dramatic impact upon the permeability of a clay-bearing sand. These effects are not directly incorporated in the present model. On the basis of the fact that the effects upon the permeability are indirectly considered in the values of the end-member shale permeability we think that the above mentioned additional effect should contribute to the order-of-magnitude variation observed between the model and data. However, this should be checked by additional tests of our model. Regarding the second question, we think that our model is applicable to the evaluation of water resources and subsurface water circulation because it is particularly suitable for determining permeability profiles from downhole measurement analysis (these permeability profiles can be integrated in basin simulators which begin to be widely used to understand subsurface hydrological circulations [e.g., *Person et al*., 1996]). The information required to determine permeability profiles from downhole measurement analysis are the following: (1) the clay mineralogy and the shale content which both can be determined from the inversion of natural radioactivity logs, (2) the grain distribution of the sand fraction which can be obtained from core samples or from downhole measurements, (3) the porosity (obtained from a lithodensity log) and a compaction model for sand shale mixtures which can also include some diagenetic effects (such as the smectite illite transformation). The development of logging tools of small diameters in the last decade makes such approaches particularly suitable in the area of water resources. A future paper will be dedicated to such a methodology.

Appendix A: The Effective Pore Radius

Bussian [1983] developed a model describing the electrical conductivity of a porous medium in which spheres of nonconducting material, representing the insulating mineral grains of a clean sand, are imbedded in a conducting material, which represents the saline water. He added surface conductivity to a model developed by *Bruggeman* [1935], *Hanai* [1960], and *Sen et al*. [1981]. Bussian's model relates the electrical conductivity of the porous medium σ, the pore fluid conductivity σ_f, and the grain surface conductivity σ_S to porosity ϕ:

$$\frac{\sigma - \sigma_S}{\sigma_f - \sigma_S}\left(\frac{\sigma_f}{\sigma}\right)^D = \phi \tag{A1}$$

where D is the "depolarizing factor." Equation (A1) can be rewritten:

$$\sigma = \sigma_f \phi^m \left(\frac{1 - \sigma_S/\sigma_f}{1 - \sigma_S/\sigma}\right)^m \tag{A2}$$

where $m \equiv 1/(1 - D)$ is the cementation exponent which appears in Archie's law, equation (6). Using the binomial expansion, the high-salinity limit ($\sigma_S/\sigma_f \ll 1$) of (A2) is

$$\sigma = \frac{1}{F}\left[\sigma_f + m(F - 1)\sigma_S\right] \tag{A3}$$

The surface conductivity σ_S is related to the specific surface conductivity Σ_S by [*Revil and Glover*, 1998] $\sigma_S = 2\Sigma_S/R$.

Comparing (7) and (A3) yields a new expression for Λ which directly involves the cementation exponent and the radius of the grains:

$$\Lambda = \frac{R}{m(F-1)} \approx \frac{R}{mF} \tag{A4}$$

Appendix B: Shale Content

The relationships between the shale content by volume φ_V and by weight φ_w is [*Marion et al*., 1992]:

$$\varphi_W = \frac{\varphi_V(1-\phi_{\mathrm{Sh}})\rho_g^{\mathrm{Sh}}}{\varphi_V(1-\phi_{\mathrm{Sh}})\rho_g^{\mathrm{Sh}} + (1-\phi_{\mathrm{Sd}})\rho_g^{\mathrm{Sd}}} \qquad \varphi_V \le \phi_{\mathrm{Sd}} \tag{B1}$$

$$\varphi_W^{\mathrm{crit}} = \frac{\phi_{\mathrm{Sd}}(1-\phi_{\mathrm{Sh}})\rho_g^{\mathrm{Sh}}}{(1-\phi_{\mathrm{Sd}})\rho_g^{\mathrm{Sd}} + \phi_{\mathrm{Sd}}(1-\phi_{\mathrm{Sh}})\rho_g^{\mathrm{Sh}}} \qquad \varphi_V = \phi_{\mathrm{Sd}} \tag{B2}$$

$$\varphi_W = \frac{\varphi_V(1-\phi_{\mathrm{Sh}})\rho_g^{\mathrm{Sh}}}{\varphi_V(1-\phi_{\mathrm{Sh}})\rho_g^{\mathrm{Sh}} + (1-\varphi_V)\rho_g^{\mathrm{Sd}}} \qquad \varphi_V \ge \phi_{\mathrm{Sd}} \tag{B3}$$

Here ρ_g^{Sh} and ρ_g^{Sd} are the grain density of clay minerals without their bound water and quartz, respectively. From (14), (15), (B1), and (B3) the porosity is obtained from φ_W by

$$\phi = \phi_{\mathrm{Sd}} - \frac{(1-\phi_{\mathrm{Sd}})\rho_g^{\mathrm{Sd}}\varphi_W}{\rho_g^{\mathrm{Sh}}(1-\varphi_W)} \qquad \varphi_W \le \varphi_W^{\mathrm{crit}} \tag{B4}$$

$$\phi = \frac{\phi_{\mathrm{Sh}}\rho_g^{\mathrm{Sd}}\varphi_W}{\rho_g^{\mathrm{Sd}}\varphi_W + (1-\phi_{\mathrm{Sh}})\rho_g^{\mathrm{Sh}}(1-\varphi_W)} \qquad \varphi_W > \varphi_W^{\mathrm{crit}} \tag{B5}$$

Appendix C: Permeability in the Sandy Shale Domain

The theoretical basis for (20) is again electrical conductivity equations for two-component mixtures. The electrical conductivity σ of a two-component mixture is given by the Bergman-Milton model [*Bergman*, 1978; *Milton*, 1980; *Korringa and La-Torraca*, 1986]:

$$\sigma = \frac{\sigma_i}{F_i} + \frac{\sigma_j}{F_j} + \int_0^\infty \left(\frac{\Theta(x)}{1/\sigma_i + x/\sigma_j} \right) dx \tag{C1}$$

where σ_i and σ_j are the electrical conductivity of the two components, F_i is the electrical formation factor found by taking all of region "i" to be the pore space and all of the region "j" to be the insulator (and symmetrically for F_j), and $\Theta(x) \ge 0$ is a resonance density which depends like $F_{i,j}$ on the topology of the two components. The integral in (C1) is known as a Stieltjes integral [*Baker*, 1975]. *Dagan* [1979] showed that the effective permeability of an inhomogeneous porous medium is determined by an equation similar to (C1) and thus that

$$k = \frac{k_i}{F_i} + \frac{k_j}{F_j} + \int_0^\infty \left(\frac{\Theta(x)}{1/k_i + x/k_j} \right) dx \tag{C2}$$

Dagan's argument is correct so long as both constituents have finite and comparable permeabilities k_i and k_j. If one of the regions is impermeable (as it would be if composed of solid grains), then the no-slip conditions arises for fluid flow (but not for electrical conductivity) and complicates the solution. However, because shale is not very permeable, the effect of the no-slip condition vanishes at very small distances from the grain surface, and consequently, this condition has only a very small influence on the overall fluid transport. Taking $k_j = 0$ in (C2) and neglecting the third term of (C2) [*Berryman*, 1992], we obtain directly (20).

Acknowledgments. We thank Pennzoil for the permeability data of the GA and HB sands and S. Losh for fruitful discussions. The project was made possible by funding from the Gas Research Institute to L. M. Cathles, funding from Elf Aquitaine to A. Revil, and the general support of the Corporate Sponsors of the Global Basin Research Network. We thank the two reviewers, E. Bekele and J. P. Raffensperger, and the Associate Editor, M. Person, for constructive reviews.

References

Avellaneda, M., and S. Torquato, Rigorous link between fluid permeability, electrical conductivity, and relaxation times for transport in porous media, *Phys. Fluids A*, *3*, 2529–2540, 1991.

Baker, G. A., Jr., *Essential of Padé Approximants*, 229 pp., Academic, San Diego, Calif., 1975.

Bear, J., *Dynamics of Fluids in Porous Media*, 764 pp., Dover, Mineola, N. Y., 1988.

Berg, R. R., Capillary pressures in stratigraphic traps, *AAPG Bull*., *59*, 939–956, 1975.

Bergman, D. J., The dielectric constant of a composite material: A problem of classical physics, *Phys. Rep*., *43*, 378–407, 1978.

Bernabé, Y., The transport properties of networks of cracks and pores, *J. Geophys. Res*., *100*, 4231–4241, 1995.

Bernabé, Y., and A. Revil, Pore-scale heterogeneity, energy dissipation and the transport properties of rocks, *Geophys. Res. Lett*., *22*, 1529–1532, 1995.

Berryman, J. G., Effective stress for transport properties in inhomogeneous porous rock, *J. Geophys. Res*., *97*, 17,409–17,424, 1992.

Bethke, C. M., Modeling subsurface flow in sedimentary basins, *Geol. Rundsch*., *78*, 129–154, 1989.

Bruggeman, D. A. G., Berechnung verschiedener physikalischer konstanten von heterogenen substanzen, *Ann. Phys*., *24*, 636–664, 1935.

Bussian, A. E., Electrical conductance in a porous medium, *Geophysics*, *48*, 1258–1268, 1983.

Chauveteau, G., and A. Zaitoun, Basic rheological behavior of xanthan polysaccharide solutions in porous media: Effect of pore size and polymer concentration, in *Enhanced Oil Recovery*, edited by F. J. Fayers, pp. 197–212, Elsevier, New York, 1981.

Chilindar, G. V., Relationship between porosity, permeability and grain size distribution of sands and sandstones, in *Deltaic and Shallow Marine Deposits*, vol. I, edited by L. M. J. U. Van Straaten, pp. 71–75, Elsevier, New York, 1964.

Dagan, G., Models of groundwater flow in statistically homogeneous porous formations, *Water Resour. Res*., *15*, 47–63, 1979. (Correction, *Water Resour. Res*., *16*, 225, 1980).

Dickey, P. A., Comment on Chocolate Bayou Field, *J. Pet. Technol*., *22*, 560–569, 1970.

England, W. A., A. S. Mackenzie, D. M. Mann, and T. M. Quigley, The movement and entrapment of petroleum fluids in the subsurface, *J. Geol. Soc. London*, *144*, 327–347, 1987.

Gondouin, M., and C. Scala, Streaming potential and the S.P. log, *J. Pet. Technol*., *10*, 170–179, 1958.

Hanai, T., Theory of the dielectric dispersion due to the interfacial polarization and its application to emulsions, *Kolloid Z*., *171*, 23–31, 1960.

Holland, D. S., J. B. Leedy, and D. R. Lammelin, Eugene Island Block 330 field: USA, offshore Louisiana, in *Compilers, Structural Traps*, vol. III, *Tectonic Fold and Fault Traps, American Association of Petroleum Geologists, Treatise of Petroleum Geology Atlas of Oil and Gas Fields*, edited by E. A. Beaumont and N. H. Foster, pp. 103–143, Am. Assoc. of Pet. Geol., Tulsa, Okla., 1990.

Johnson, D. L., T. J. Plona, C. Scala, F. Pasierb, and H. Kojima, Tortuosity and acoustic slow waves, *Phys. Rev. Lett*., *49*, 1840–1844, 1982.

Johnson, D. L., T. J. Plona, and H. Kojima, Probing porous media with 1st sound, 2nd sound, 4th sound and 3rd sound, in *Physics and Chemistry of Porous Media*, vol. II, edited by R. Jayanth, J. Banavar, and K. W. Winkler, pp. 243–277, AIP, New York, 1986.

Knoll, M. D., and R. Knight, Relationships between dielectric and hydrogeologic properties of sand-clay mixtures, paper presented at Fifth International Conference on Ground Penetrating Radar, Kitchener, Ontario, 1994.

Koltermann, C. E., and S. M. Gorelick, Fractional packing model for hydraulic conductivity derived from sediment mixtures, *Water Resour. Res*., *31*, 3283–3297, 1995.

Korringa, J., and G. A. LaTorraca, Application of the Bergman-Milton theory of bounds to the permittivity of rocks, *J. Appl. Phys*., *60*, 2966–2976, 1986.

Kostek, S., L. M. Schwartz, and D. L. Johnson, Fluid permeability in porous media: Comparison of electrical estimates with hydrodynamical calculations, *Phys. Rev. B*, *45*, 186–195, 1992.

Krohn, C. E., Fractal measurements of sandstones, shales, and carbonates, *J. Geophys. Res*., *93*, 3297–3305, 1988.

Marion, D., A. Nur, H. Yin, and D. Han, Compressional velocity and porosity in sand-clay mixtures, *Geophysics*, *57*, 554–563, 1992.

Matlack, K. S., D. W. Houseknech, and K. R. Applin, Emplacement of clay into sand by infiltration, *J. Sediment. Petrol*., *59*, 77–87, 1988.

Mendelson, K. S., and M. H. Cohen, The effects of grain anisotropy on the electrical properties of sedimentary rocks, *Geophysics*, *47*, 257–263, 1982.

Mesri, G., and R. E. Olson, Mechanisms controlling the permeability of clays, *Clays Clay Miner*., *19*, 151–158, 1971.

Milton, G. W., Bounds on the complex dielectric constant of a composite material, *Appl. Phys. Lett*., *37*, 300–303, 1980.

Moore, D. E., C. A. Morrow, and J. D. Byerlee, Use of swelling clays to reduce permeability and its potential application to nuclear waste repository sealing, *Geophys. Res. Lett*., *9*, 1009–1012, 1982.

Nelson, P. H., Permeability-porosity relationships in sedimentary rocks, *Log Analyst*, May-June, 38–62, 1994.

Olsen, H. W., Darcy's law in saturated kaolinite, *Water Resour. Res*., *2*, 287–294, 1966.

Pape, H., L. Riepe, and J. R. Schopper, Interlayer conductivity of rocks: A fractal model of interface irregularities for calculating interlayer conductivity of natural porous mineral systems, *Colloids Surf*., *27*, 97–122, 1987.

Patchett, J. G., An investigation of shale conductivity, paper presented at 16th Annual Logging Symposium, Soc. of Prof. Well Log Analysts, New Orleans, La., 1975.

Person, M., J. P. Raffensperger, S. Ge, and G. Garven, Basin-scale hydrogeologic modeling, *Rev. Geophys*., *34*, 61–87, 1996.

Revil, A., and P. W. J. Glover, Theory of ionic-surface electrical conduction in porous media, *Phys. Rev. B*, *55*, 1757–1773, 1997.

Revil, A., and P. W. J. Glover, Nature of surface electrical conductivity in natural sands, sandstones, and clays, *Geophys. Res. Lett*., *25*, 691–694, 1998.

Revil, A., L. M. Cathles, S. Losh, and J. A. Nunn, Electrical conductivity in shaly sands with geophysical applications, *J. Geophys. Res*., in press, 1998a.

Revil, A., L. M. Cathles III, J. D. Shosa, P. A. Pezard, and F. D. de Larouzière, Capillary sealing in sedimentary basins: A clear field example, *Geophys. Res. Lett*., *25*, 389–392, 1998b.

Rowlands, W. N., R. W. O'Brien, P. J. Hunter, and V. Patrick, Surface properties of aluminium hydroxide at high salt concentration, *J. Colloid Interface Sci*., *188*, 325–335, 1997.

Schwartz, L. M., P. N. Sen, and D. L. Johnson, Influence of rough surfaces on electrolytic conduction in porous media, *Phys. Rev. B*, *40*, 2450–2458, 1989.

Sen, P. N., C. Scala, and M. H. Cohen, Self similar model for sedimentary rocks with application to the dielectric constant of fused glass beads, *Geophysics*, *46*, 781–795, 1981.

Von Engelhardt, W., and K. H. Gaida, Concentration changes of pore solutions during the compaction of clay sediments, *J. Sediment. Petrol*., *33*, 919–930, 1963.

Walsh, J. B., and W. F. Brace, The effect of pressure on porosity and the transport properties of rock, *J. Geophys. Res*., *89*, 9425–9431, 1984.

Waxman, M. H., and L. J. M. Smits, Electrical conductivities in oil-bearing shaly sands, *Soc. Pet. Eng. J*., *8*, 107–122, 1968.

Whitworth, T. M., and S. J. Fritz, Electrolyte-induced solute permeability effects in compacted smectite membranes, *Appl. Geochem*., *9*, 553–546, 1994.

Wintsch, R. P., R. Christoffersen, and A. K. Kronenberg, Fluid-rock reaction weakening of fault zones, *J. Geophys. Res*., *100*, 13,021–13,032, 1995.

L. M. Cathles III, Global Basin Research Network Group, Department of Geological Sciences, Cornell University, Ithaca, NY 14853.

A. Revil, Department of Geophysics, CEREGE, BP 80, 13545 Aix-en-Provence, Cedex 4, France. (revil@cerege.fr)

(Received October 27, 1997; revised August 14, 1998;
accepted August 17, 1998.)